Controlling the transverse momentum distribution of a light field via azimuth division of a hologram in holographic optical tweezers

Sheng-Yang Tseng* and Long Hsu

Department of Electrophysics, National Chiao Tung University, 1001 University Road, Hsinchu, Taiwan 300

*Corresponding author: tws.ep93g@nctu.edu.tw

Received 6 June 2011; revised 3 September 2011; accepted 9 September 2011; posted 14 September 2011 (Doc. ID 148755); published 10 November 2011

This study proposes a method for creating a light field with controlled distribution of transverse momentum (TM) by displaying a hologram only in an azimuth region that centers at θ_0 and has a range of $\Delta\theta$ of a spatial light modulator in holographic optical tweezers. This study utilized ray optics to analyze the TM of the resultant field, revealing that the direction of the TM is determined by the center angle of the azimuth region and that the magnitude of the TM is proportional to $\sin(\Delta\theta/2)$, without regarding the intensity. The relationship was verified experimentally. In addition, this study demonstrated moving particles along a designed path and depleting particles by the fields.

OCIS codes: 140.7010, 090.1760, 230.6120.

1. Introduction

Using holographic optical tweezers (HOTs) [1–4] to create a light field with momentum transverse to the optical axis provides a simpler approach for controlling the motions of microparticles. Without any light intensity change or external force, particles in the field can move along the region of highest intensity because of the transverse momentum (TM). A large number of applications have thus utilized special light modes with the TM, such as optical vortices. [5–7]. Studies of creating a light field with a controlled distribution of momentum have been conducted as well [8–12].

In electromagnetic theory, the TM of a field is proportional to the phase gradient and intensity of the field [13]. Applying only phase modulation to a light field is insufficient to control the TM distribution. Certain studies adjust both the amplitude and phase of a light field to produce a desired TM distribution. For instance, the shape-phase algorithm [10] by Roichman and Grier uses a phase-only hologram to direct partial light with assigned phase shifts, according to a shape function that produces a required amplitude distribution. Another method, proposed by Jesacher *et al.* [11], is based on controlling amplitude and phase distribution with two cascade phase-only holograms.

In ray optics, models of light fields are composed of rays. Because the momentum of a ray rests along the ray's direction, inclined rays contribute the TM [14]. In conventional optical tweezers [15], numerous inclined rays are created when incident rays are brought into focus. However, because of the azimuth symmetry of incident light intensity, the TM contributed by the incident rays is cancelled out completely at the focus. This implies that breaking the azimuth symmetry can realize alternative approaches toward creating a light field with TM distribution.

Based on this notion, this study proposes a method for creating a light field with a controlled TM distribution by displaying a hologram only in an azimuth region of a spatial light modulator (SLM) in HOTs. This paper uses ray optics to analyze the TM distribution of the resultant field. By tracing all the

0003-6935/11/340H62-06$15.00/0

incident rays from the SLM to the focal plane of an objective in HOTs and summing the TM contributed by all the rays passing through the same points of the focal plane, the TM distribution of the field can be obtained. Implementation of this approach reveals a criterion for creating a light field with a controlled TM distribution. To verify the proposed method, electromagnetic theory is used to calculate the TM distributions of resultant fields numerically. In addition, the ability of moving particles of these fields is experimentally demonstrated.

2. Theory

This section presents the usage of ray optics to analyze the TM flux density, the TM per unit time per unit area, of an optical pattern produced by a hologram that is displayed only in an azimuth region of an SLM in HOTs. The azimuth region centers at θ_0 and has an angle range of $\Delta\theta$. A normally incident, collimated ray bundle of power p_{total} that extends over the entire input aperture of an objective models the incident light. Before considering the diffraction effect of the hologram, the TM flux at focus is analyzed, to which all of the incident rays within the azimuth region converge.

In HOTs, a hologram displayed on an SLM is imaged onto the back focal plane of an objective. The resultant light field is consequently created on the front focal plane of the objective. Thus, the setup of HOTs can be simplified to an objective between the front and back focal planes. A typical objective used in HOTs is an infinite-corrected objective, which conforms to the Abbe sine condition, and can be modeled by the first principal plane (PP), the second PP, and a spherical surface S [16]. The spherical surface S is centered at the focus, and is a tangent to the second PP.

Figure 1 shows the path of a normally incident ray in HOTs from the SLM plane through an objective to the focal plane. The optical axis is in the z direction. The ray originates from the azimuth region at the position $\mathbf{r_r} = r_r\cos(\theta)\mathbf{x} + r_r\sin(\theta)\mathbf{y}$ and crosses the first PP at Point A_1, which is at the same position $\mathbf{r_r}$. According to the Abbe sine condition [16], the ray emerges from Surface S at Point A_s, of which the transverse component of the position vector is also $\mathbf{r_r}$, before converging to the focus. At the focus, the TM flux contributed by the ray $P_{t,\text{ray}}$ can be shown as follows:

$$\begin{aligned}\mathbf{P}_{\mathbf{t,ray}} &= -\left(\frac{np_{\text{ray}}}{cf_{\text{obj}}}\right)\mathbf{r_r} \\ &= -\left(\frac{np_{\text{ray}}}{cf_{\text{obj}}}\right)r_r[\cos(\theta)\mathbf{x} + \sin(\theta)\mathbf{y}], \end{aligned} \tag{1}$$

where n is the refractive index of the surroundings, p_{ray} is the power transported by the ray, c is the speed of light in vacuum, f_{obj} is the focal length of the objective, and $\mathbf{x}$ and $\mathbf{y}$ are the unit vectors in the x and y direction, respectively. Since all the normal incident rays within the azimuth region converge to the focus, after summing, or integrating, the TM contributed by all the rays within the region, the total TM at the focus $\mathbf{P}_{\mathbf{t,total}}^{p_{total}}$ can be obtained by

$$\begin{aligned}\mathbf{P}_{\mathbf{t,total}}^{p_{\text{total}}} &= \int_0^R \int_{\theta_0-\Delta\theta/2}^{\theta_0+\Delta\theta/2} N_r\mathbf{P}_{\mathbf{t,ray}} r_r \mathrm{d}\theta\mathrm{d}r_r \\ &= -\int_0^R \int_{\theta_0-\Delta\theta/2}^{\theta_0+\Delta\theta/2} N_r\left(\frac{n}{cf_{\text{obj}}}\right)\left(\frac{p_{\text{total}}}{\pi R^2 N_r}\right) \\ &\quad\times[\cos(\theta)\mathbf{x} + \sin(\theta)\mathbf{y}]r_r^2\mathrm{d}\theta\mathrm{d}r_r \\ &= -\left(\frac{2}{3\pi c}\right)\left(n\frac{R}{f_{\text{obj}}}\right)p_{\text{total}}\sin(\Delta\theta/2) \\ &\quad\times[\cos(\theta_0)\mathbf{x} + \sin(\theta_0)\mathbf{y}], \end{aligned} \tag{2}$$

where R is the radius of the objective's back aperture, N_r is number density of the incident rays on the SLM, and p_{ray} is substituted by $p_{\text{total}}/(\pi R^2 N_r)$.

When considering the diffraction effect of the hologram, the incident ray bundle is assumed to be split into a large number of collimated ray bundles bearing different headings and power after the hologram. This is similar to the concept of the angular spectrum in Fourier optics [17], which decomposes a field into plane waves, though these ray bundles originate only from the azimuth region. Once these ray bundles pass through the objective, they converge to points

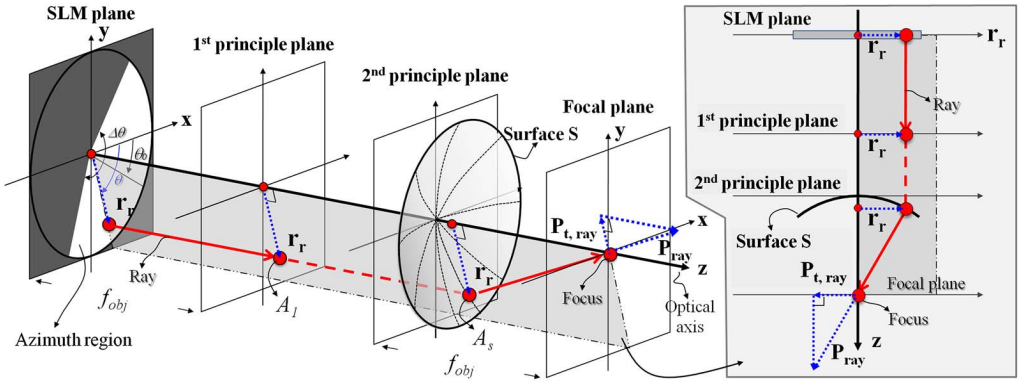

Fig. 1. (Color online) Schematic illustration of a ray path in HOTs from the SLM plane to the focal plane.

on the focal plane and form an intensity distribution $I(x,y)$.

Usually, the size of the optical pattern is significantly smaller compared to the focal length of the objective. The inclined angles between the ray bundles and the optical axis are close to zero. This study thus assumes that regardless of the inclined angles, these ray bundles contribute the same TM flux at the focal plane as long as they have the same power. In other words, the total TM flux of the entire optical pattern is equal to the TM flux at the focus to which all the incident rays converge. Consequently, the TM flux density of the optical pattern $\mathbf{J}_{\mathbf{total}}^{p_{\text{total}}}(x,y)$ can be obtained by redistributing the total TM at the focus to the entire optical pattern according to the intensity distribution, as follows:

$$\mathbf{J}_{\mathbf{total}}^{p_{\text{total}}}(x,y) = \mathbf{P}_{\mathbf{t,total}}^{p_{\text{total}}} I_n(x,y), \tag{3}$$

where

$$I_n(x,y) = \frac{I(x,y)}{\int_{-\infty}^{\infty}\int_{-\infty}^{\infty} I(x,y)\mathrm{d}x\mathrm{d}y}, \tag{4}$$

which is a normalized intensity distribution of the optical pattern. After substituting Eq. (2) into Eq. (3), the TM flux density of the optical pattern becomes

$$\mathbf{J}_{\mathbf{t,total}}^{p_{\text{total}}}(x,y) = -\left(\frac{2}{3\pi c}\right)\left(n\frac{R}{f_{\text{obj}}}\right)p_{\text{total}}\sin(\Delta\theta/2) \times [\cos(\theta_0)\mathbf{x} + \sin(\theta_0)\mathbf{y}] I_n(x,y). \tag{5}$$

From Eq. (5), the direction of the TM flux density is along $-[\cos(\theta_0)\mathbf{x} + \sin(\theta_0)\mathbf{y}]$, which is determined only by θ_0. The magnitude of the TM flux density is proportional to the normalized intensity $I_n(x,y)$ and the total incident power p_{total}. In addition, the magnitude of the TM flux density is also proportional to $\sin(\Delta\theta/2)$. When $\Delta\theta$ is equal to 0°, the TM flux density is zero due to an absence of incident rays. As $\Delta\theta$ increases, the magnitude of the TM flux density increases in conjunction with the extension of the azimuth region, reaching its maximum value at $\Delta\theta = 180°$. However, when $\Delta\theta$ is larger than 180°, more rays arrive at the focal plane, though part of the TM flux density is cancelled by the newly added rays. The magnitude of the TM flux density thus decreases and experiences a complete cancellation when $\Delta\theta = 360°$. This is the reason why the TM flux, or the transverse scattering force, is not observed in optical tweezers.

Creating an optical pattern with controlled TM distribution thus becomes two parts: (1) controlling the direction of the TM by adjusting θ_0 of an azimuth region with $\Delta\theta < 360°$; and (2) calculating a required hologram for producing a desired intensity distribution, which can be accomplished by most algorithms used in HOTs, such as the Gerchberg–Saxton (GS) algorithm [18], the weighted GS algorithm (GSW) [19], or the generalized adaptive add algorithm (GAA) [3].

3. Setup

The schematic illustration of the experimental setup is shown in Fig. 2. The trapping laser is a fiber laser (YLR-10-1064-LP; IPG photonics) with an output power of up to 10 W at 1064 nm. The laser beam is first expanded by a beam expander to fulfill the active area of the SLM (X10468-03; Hamamatsu). A half-wave plate and a polarized beam splitter are utilized to control incident laser power on the SLM. The laser beam immediately leaving the SLM is consequently imaged by a telescope onto the back focal plane of a 100× water-immersion objective, with a numerical aperture (NA) that equals 1.1 (Plan; Nikon). Once the laser beam passes through the objective, a designed optical field is formed on a sample held on a stage. The sample is illuminated by a light-emitting diode (LED) and is imaged on a CCD camera (PL-B955G; PixeLink) by the objective and a tube lens.

4. Results

Figure 3(a) shows a phase-only hologram for producing two trap arrays with opposite directions of TM. The hologram is divided into two azimuth regions, separated by a horizontal dash line. The hologram in each region produces a point trap array labeled with the same number as that of the azimuth region, as shown in Fig. 3(b). The trap arrays extend in the y direction. The traps in each trap array are arranged to set the distances between the neighboring traps at 2 μm. According to Eq. (5), the central angle of Region 1 is 90°; the TM of the resultant trap array is therefore along $-\mathbf{y}$. Similarly, the central angle of Region 2 is 270°; the TM of the resultant trap array is hence along $\mathbf{y}$.

Figures 3(c) and 3(d) show the normalized simulated TM distributions of the resultant field in the x and y directions, respectively. The field produced by the hologram was calculated by performing a fast Fourier transform (FFT) on the transmittance of the

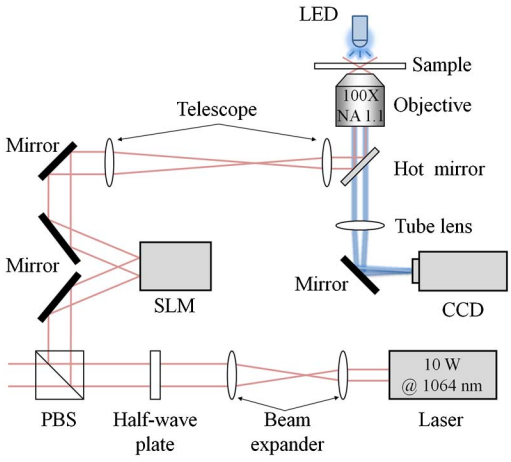

Fig. 2. (Color online) Experimental setup.

hologram. The TM distribution of the field was subsequently calculated by multiplying the intensity distribution by the gradient of the phase distribution of the field [13] before normalizing by the maximum magnitude of the result. These figures show that the TM of the trap array produced by Region 1 is along **–y**, indicated by a black color, and that of the trap array produced by Region 2 is along **y**, indicated by a white color. These results are consistent with the results predicted by Eq. (5).

These trap arrays were projected in a solution of 9 μm diameter polystyrene beads, which was placed between a cover slip and a slide. Figure 3(e) shows the sequential snapshots of beads moving along the trap arrays. The beads were pushed against the slide surface and were confined in the trap arrays. Within the trap arrays, the beads experienced only light gradient force due to cancellation between the gradient forces from different traps. As the beads scattered the photons of the trap array, they obtained the TM and thus moved along the y direction. Equation (5) shows that the TM is proportional to $\sin(\Delta\theta/2)$ and p_{total}; the average moving speeds of the beads should thus also be proportional to $\sin(\Delta\theta/2)$ and p_{total}.

Figure 4(a) shows the average moving speed in the y direction of the beads in the trap arrays at different $\Delta\theta$ and p_{total}. The solid lines are a result of the fits to the function $V_{\max}\sin(\Delta\theta/2)$, where $V_{\max}$ is a free parameter. The data show the same dependence

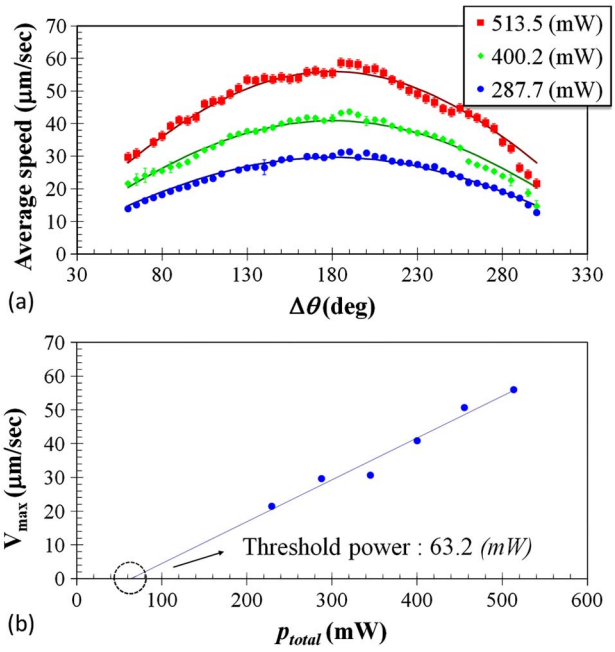

Fig. 4. (Color online) Average moving speed of a 9 μm diameter bead in a trap array at different $\Delta\theta$ and p_{total}: (a) is the average moving speed at different $\Delta\theta$ from 60° to 300°. The solid lines fit the function $V_{\max}\text{Sin}(\Delta\theta/2)$; (b) is $V_{\max}$ at different incident power p_{total}. The straight line is a linear fit, which does not pass through the origin, indicating that a minimum incident power of approximately 63.2 mW is required to overcome the resistance between the particle and slide surface.

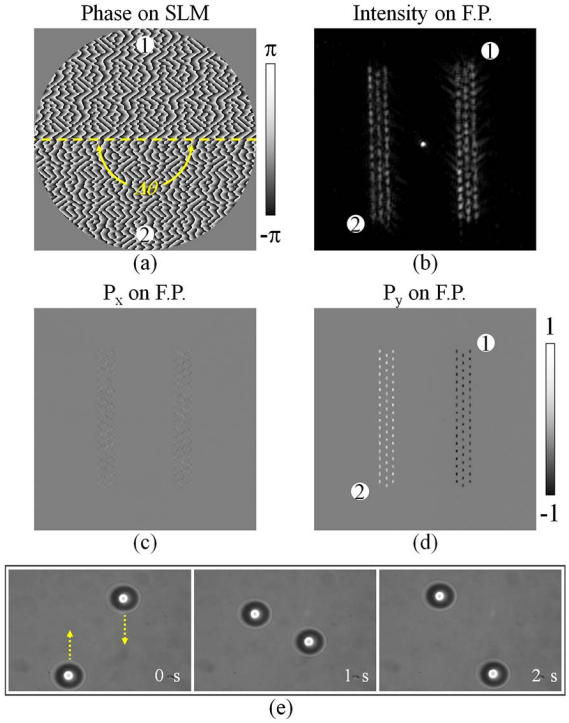

Fig. 3. (Color online) Moving particles along two trap arrays (a number near the trap array indicates the region from which the trap array was created): (a) is the phase pattern for creating two trap arrays; (b) is the corresponding intensity distribution on the focal plane; (c) and (d) are the simulated TM distributions in the x and y directions, respectively; and (e) represents the sequential snapshots of two 9 μm diameter beads moving in the trap arrays.

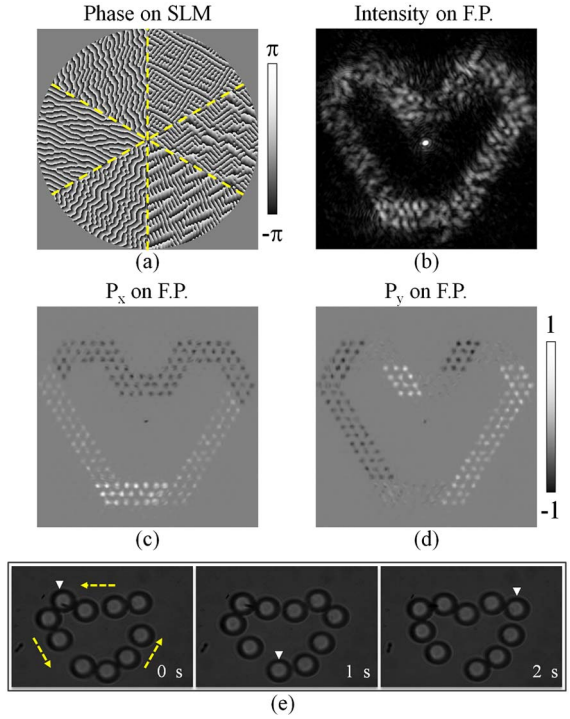

Fig. 5. (Color online) Particles moving along a heart-shaped path: (a) is the phase pattern for producing a heart-shaped path; (b) is the corresponding intensity distribution on the focal plane; (c) and (d) are the simulated TM distributions in the x and y directions, respectively; and (e) represents the sequential snapshots of beads moving along the path (Media 1).

on $\Delta\theta$ as the TM flux density predicted by Eq. (5). Figure 4(b) shows V_{max} at different p_{total}. The solid line is a linear fit and does not pass through the origin, indicating that a minimum input power of approximately 63.2 mW is required to move the beads. This may be caused by the resistance between the surface and the beads.

A more complex path can also be created. A phase pattern which produces point traps that form a heart-shaped path is shown in Fig. 5(a). The traps are arranged to set the direction of TM along the path. The corresponding intensity and the simulated TM distributions in the x and y directions are shown in Figs. 5(b)–5(d). Figure 5(e) (Media 1) represents the sequential snapshots of moving 9 μm diameter beads along the path. The time interval between snapshots is 1 s. The white triangle in each snapshot indicates the same bead at different times. These figures show that the beads move along the path in a direction, as predicted by the simulated results.

In addition to moving particles along closed loops, trap arrays can also be used to deplete particles. Figure 6(a) shows a phase pattern for producing an equally-spaced trap array with 2 μm spacing, which forms a hexagon. The phase pattern is divided into six regions. The phase pattern in each region produces a triangular trap array, which is labeled with the same number as the corresponding region, shown in Fig. 6(b). The TM of these triangular trap arrays directs outward from the center of the hexagon, as shown in Figs. 6(c) and 6(d). Figure 6(e) (Media 2) represents the sequential snapshots when the trap array was projected in a solution containing 0.5 μm diameter beads. The time interval between snapshots is 1 s. At the beginning of the experiment, a large number of beads were located in the center of the screen. Over time, the beads jumped outward because of the TM and help from Brownian motions and particle collisions. When most particles were outside the trap array, particle collisions became rare. The Brownian motions of particles became the only aid for the particles to overcome the gradient forces. The depletion rate thus decreased and some particles remained trapped at the end of the experiment. This process can be reversed with the reversal of the direction of the TM in each subtrap array. In this manner, particles can be concentrated at the central region and local particle concentration can thus be controlled.

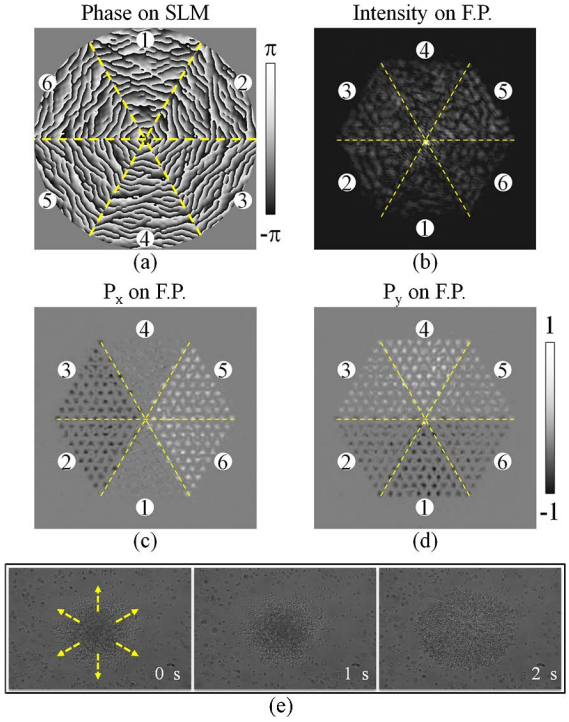

Fig. 6. (Color online) Depleting 0.5 μm diameter beads by an equally-spaced trap array with TM directing outward (a number near each triangular trap array indicates the azimuth region from which the triangular trap array was created): (a) is the phase pattern for producing an equally-spaced trap array, which forms a hexagon; (b) is the corresponding intensity distribution on the focal plane; (c) and (d) are the simulated TM distributions in the x and y directions, respectively; and (e) represents the sequential snapshots of bead depletion (Media 2).

5. Conclusion

This paper proposes an alternative method for controlling the TM distribution of a light field, other than by modulating its phase and amplitude distribution. This study used ray optics to analyze the TM distribution of a field produced by a hologram. The results reveal that a field with controlled TM distribution can be created by displaying a hologram only in an azimuth region with an angle range of $\Delta\theta < 360°$. The direction of the resultant TM distribution is determined by the center angle θ_0 and lies along the direction $-[\cos(\theta_0)\mathbf{x} + \sin(\theta_0)\mathbf{y}]$. The magnitude of the TM is proportional to $\sin(\Delta\theta/2)$, without regarding the intensity distribution of the field. The control of the TM distribution of a light field is thus divided into two parts: (1) controlling the direction of the TM by adjusting θ_0 of an azimuth region with $\Delta\theta < 360°$; and (2) calculating a required hologram to produce a desired intensity distribution.

The relationship is experimentally verified. In addition, this study created point trap arrays with controlled TM distributions to demonstrate moving particles along predetermined paths and the depletion of particles.

The authors thank Sien Chi and Yi-Ren Chang for their thought-provoking discussions and suggestions.

References

1. M. Reicherter, T. Haist, E. U. Wagemann, and H. J. Tiziani, "Optical particle trapping with computer-generated holograms written on a liquid-crystal display," Opt. Lett. **24**, 608–610 (1999).
2. J. Liesener, M. Reicherter, T. Haist, and H. J. Tiziani, "Multi-functional optical tweezers using computer-generated holograms," Opt. Commun. **185**, 77–82 (2000).
3. J. E. Curtis, B. A. Koss, and D. G. Grier, "Dynamic holographic optical tweezers," Opt. Commun. **207**, 169–175 (2002).

4. A. Jesacher, S. Furhapter, S. Bernet, and M. Ritsch-Marte, "Diffractive optical tweezers in the Fresnel regime," Opt. Express **12**, 2243–2250 (2004).
5. A. Jesacher, S. Furhapter, C. Maurer, S. Bernet, and M. Ritsch-Marte, "Holographic optical tweezers for object manipulations at an air-liquid surface," Opt. Express **14**, 6342–6352 (2006).
6. K. Ladavac and D. G. Grier, "Microoptomechanical pumps assembled and driven by holographic optical vortex arrays," Opt. Express **12**, 1144–1149 (2004).
7. J. Plewa, E. Tanner, D. M. Mueth, and D. G. Grier, "Processing carbon nanotubes with holographic optical tweezers," Opt. Express **12**, 1978–1981 (2004).
8. J. Lin, X. C. Yuan, S. H. Tao, X. Peng, and H. B. Niu, "Deterministic approach to the generation of modified helical beams for optical manipulation," Opt. Express **13**, 3862–3867 (2005).
9. J. E. Curtis and D. G. Grier, "Modulated optical vortices," Opt. Lett. **28**, 872–874 (2003).
10. Y. Roichman and D. G. Grier, "Projecting extended optical traps with shape-phase holography," Opt. Lett. **31**, 1675–1677 (2006).
11. A. Jesacher, C. Maurer, A. Schwaighofer, S. Bernet, and M. Ritsch-Marte, "Full phase and amplitude control of holographic optical tweezers with high efficiency," Opt. Express **16**, 4479–4486 (2008).
12. E. R. Shanblatt and D. G. Grier, "Extended and knotted optical traps in three dimensions," Opt. Express **19**, 5833–5838 (2011).
13. Y. Roichman, B. Sun, Y. Roichman, J. Amato-Grill, and D. G. Grier, "Optical forces arising from phase gradients," Phys. Rev. Lett. **100**, 013602 (2008).
14. S. Y. Tseng and L. Hsu, "An intuitive view of the origin of orbital angular momentum in optical vortices," Proc. SPIE **6326**, 63261C (2006).
15. A. Ashkin, J. M. Dziedzic, J. E. Bjorkholm, and S. Chu, "Observation of a single-beam gradient force optical trap for dielectric particles," Opt. Lett. **11**, 288–290 (1986).
16. M. Mansuripur, *Classical Optics and its Applications* (Cambridge University Press, 2002).
17. J. W. Goodman, *Introduction to Fourier Optics*, 3rd ed. (McGraw-Hill, 1996).
18. R. W. Gerchberg and W. O. Saxton, "A practical algorithm for the determination of phase from image and diffraction plane pictures," Optik **35**, 237–246 (1972).
19. R. Di Leonardo, F. Ianni, and G. Ruocco, "Computer generation of optimal holograms for optical trap arrays," Opt. Express **15**, 1913–1922 (2007).